Journal of Inorganic Biochemistry 193 (2019) 52–59

Contents lists available at ScienceDirect

Journal of Inorganic Biochemistry

journal homepage: www.elsevier.com/locate/jinorgbio

Syntheses, crystal structures and biological evaluation of two new Cu(II) and Co(II) complexes based on (*E*)-2-(((4H-1,2,4-triazol-4-yl)imino)methyl)-6-methoxyphenol

Shao-Mei Zhang[a,1], Hai-Yang Zhang[a,1], Qi-Pin Qin[b,*], Jia-Wei Fei[a], Shu-Hua Zhang[a,*]

[a] *Guangxi Key Laboratory of Electrochemical and Magnetochemical Functional Materials, College of Chemistry and Bioengineering, Guilin University of Technology, Guilin 541004, China*

[b] *Guangxi Key Lab of Agricultural Resources Chemistry and Biotechnology, College of Chemistry and Food Science, Yulin Normal University, 1303 Jiaoyudong Road, Yulin 537000, PR China*

ARTICLE INFO

InChIKeys:
JJYFTRHRCGBJBH-MWGJFSEKSA-J
AVJRESFOXUJARJ-MWGJFSEKSA-J*Keywords:*
(*E*)-2-(((4H-1,2,4-triazol-4-yl)imino)methyl)-6-methoxyphenol
Cu(II) complex
Cell apoptosis
Mitochondrial dysfunction
Cell cycle

ABSTRACT

Two transition metal complexes of $[M(TMP)_2(H_2O)_2]$ (**TMP-Cu**, M = Cu; **TMP-Co**, M = Co) with (*E*)-2-(((4H-1,2,4-triazol-4-yl)imino)methyl)-6-methoxyphenol (H-TMP) were first synthesized and characterized by infrared analysis, elemental analysis and single crystal X-ray diffraction analysis. Notably, MTT (3-(4,5-dimethylthiazol-2-yl)-2,5-diphenyltetrazolium bromide) assay showed that **TMP-Cu** displayed relatively high cytotoxic activity against Hep-G2 cancer cells, and high selectivity between human hepatocellular carcinoma cells and normal HL-7702 cells, in comparison to **TMP-Co** and cisplatin. Further studies showed that **TMP-Cu** and **TMP-Co** caused cell cycle arrest at S phase through regulation of S phase related protein expressions and induced Hep-G2 cell apoptosis via the mitochondrial pathway.

1. Introduction

Metal complexes have been studied as potential chemotherapeutic agents to reduce side effects and resistance caused by cisplatin since cisplatin was discovered and successfully used in clinical applications [1–13]. However, these metal complexes are mostly based on precious metals such as ruthenium, platinum, and palladium compounds. Yet, other d-block complexes have been used as materials for novel metal-based drugs [14]. For example, nickel complexes have been shown as important complexes, and Ni enzymes play key roles in nitrogen, carbon, and oxygen cycles [15]. Cobalt is also an important bioelement which revealed physiological function through B_{12}. Cu complexes are efficacious anticancer agents [16–20]. In recent years, copper complexes have undergone tremendous research and development because many copper complexes are used as medicine [16–23]. As is well known, 4H-1,2,4-triazole has good biological activity [24]. Further, many Schiff bases and their metal complexes have been used as medical materials because they have excellent biological properties. In medical research, copper compounds which were constructed by Schiff bases have been proven as an attractive field [20,22]. Recently, our group reported Cd- or Zn-polymers of (*E*)-2-(((4H-1,2,4-triazol-4-yl) imino) methyl)-4,6-dihalogenphenol [25]. However, the Schiff base metal complex of (*E*)-2-(((4H-1,2,4-triazol-4-yl)imino)methyl)-6-methoxyphenol (H-TMP) derived from 4H-1,2,4-triazol-4-amine and 2-Hydroxy-3-methoxy-benzaldehyde has not been reported until now. Herein, two new $[M(TMP)_2(H_2O)_2]$ (**TMP-Cu**, M = Cu; **TMP-Co**, M = Co) complexes with (*E*)-2-(((4H-1,2,4-triazol-4-yl)imino)methyl)-6-methoxyphenol (H-TMP) ligand, were synthesized and characterized by IR, elemental analysis and single crystal X-ray diffraction analysis. The biology activity and mechanisms of action of **TMP-Cu** and **TMP-Co** were studied.

2. Results and discussion

2.1. Crystal structures

Single-crystal X-ray diffraction analysis revealed that **TMP-Cu** and **TMP-Co** were isomorphic complexes (Fig. 1), and the crystal system and space group of **TMP-Cu** and **TMP-Co** were identical. Additionally, they represent the first (*E*)-2-(((4H-1,2,4-triazol-4-yl)imino)methyl)-6-methoxyphenol (H-TMP) complexes. Therefore only complex **TMP-Cu** was analyzed here.

* Corresponding authors.
E-mail addresses: zsh720108@163.com (S.-H. Zhang), qpqin2018@126.com (Q.-P. Qin).
[1] These authors contributed equally to this work.

https://doi.org/10.1016/j.jinorgbio.2019.01.009
Received 3 November 2018; Received in revised form 10 January 2019; Accepted 12 January 2019
Available online 15 January 2019
0162-0134/

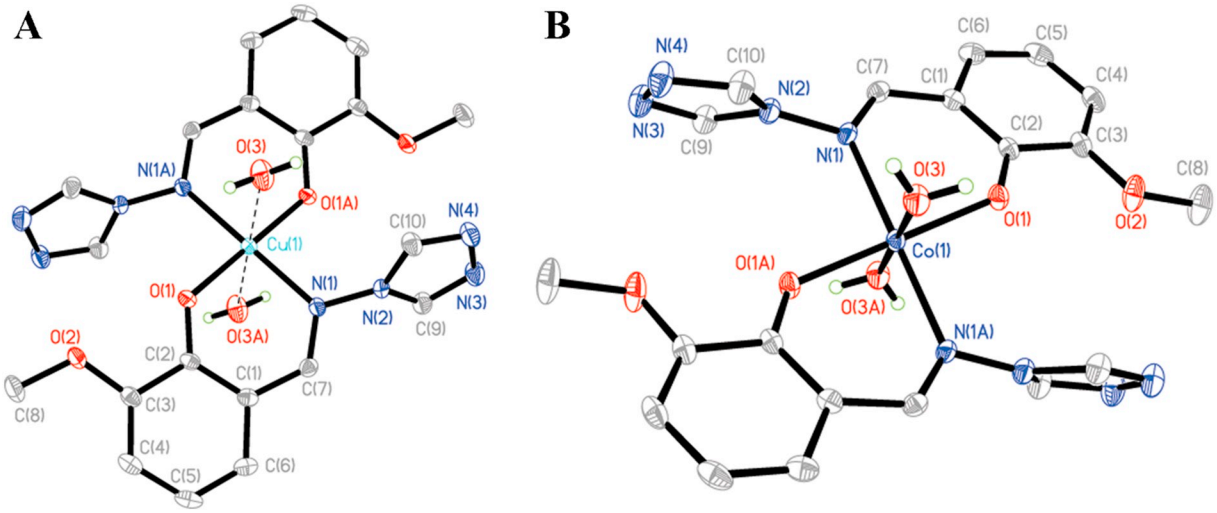

Fig. 1. Molecule structures of **TMP-Cu** (A) and **TMP-Co** (B).

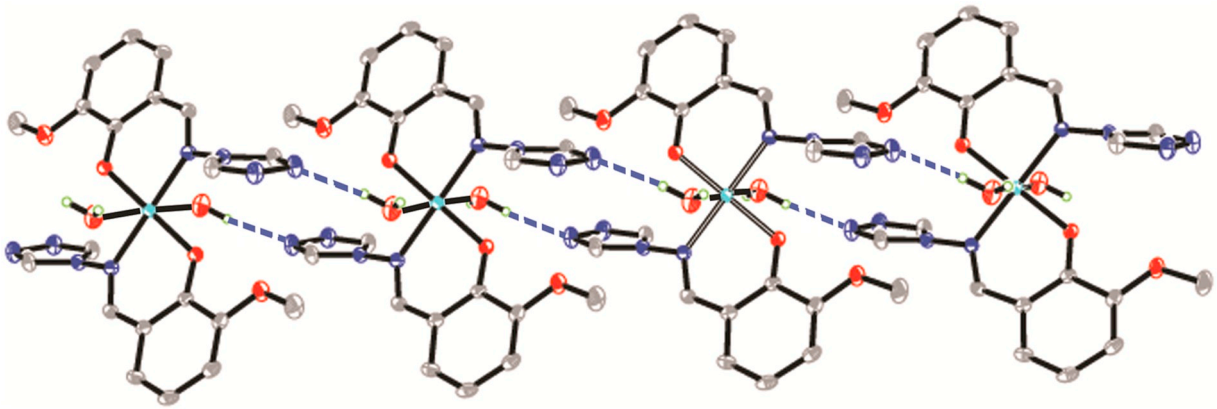

Fig. 2. 1-D chain of **TMP-Cu**.

Single-crystal X-ray diffraction analysis revealed that **TMP-Cu** belonged to the monoclinic space group $P2_1/c$. The Cu1 was six-coordinated by two O and two N atoms (O1, O1a, N1, N1a) from two different TMP ligands and two water (H_2O) molecules forming slightly distorted octahedral geometry. The bond distances of Cu1-O1, and Cu1-N1 were 1.904(2) and 2.001(2) Å, respectively. The Cu1-O3 distance was 2.483(2) Å. It is very interesting that the bond length difference around Cu1 may be caused by the Jahn-Teller effect [26–29]. It must be noted that the TMP ligand displayed the μ-TMP-κ^2O^1,N^1 coordination mode (Figs. 1, 2), which is different than the coordination mode of $[Zn(L)_2]_n$ (HL is (*E*)-2-(((4H-1,2,4-triazol-4-yl)imino)methyl)-4,6-dihalogenphenol) [25]. Further, the three coordination atoms (O2, N3, N4) of the TMP ligand were not involved in coordination.

The complex **TMP-Cu** formed a 1-D chain through double O—H···N hydrogen bonds (O3—H3B···N3^{i} 2.827(3) Å, symmetry code: (i) x, y, $z-1$. Fig. 2) which further constructed a 2-D network through abundant O—H···N and C—H···O hydrogen bonds (O3—H3A···N4^{ii} 2.942(3) Å, C9—H9A···O2^{iii} 3.269(3) Å, symmetry code: (ii) x, $0.5-y$, $z-0.5$, (iii) x, y, $z+1$, Fig. S1). It must be noted that the 2-D network formed a 3-D network through weak π···π interaction (π···π^{iv}, 3.419(2) Å, symmetry code: (iv) $-x$, $1-y$, $-z-1$).

2.2. Hirshfeld surface and fingerprint plot analysis

Hirshfeld surface analysis employed 3-D molecular surface contours in the crystal structure and was performed to visualize the different intermolecular interactions [25–29]. For a particular compound, Hirshfeld surfaces of the crystal structure were constructed based on the electron distribution, which was calculated as the sum of spherical atom electron densities.

The 2-D fingerprint plot is one of the important supplements for Hirshfeld surface analysis and was used to quantitatively analyze the nature and type of intermolecular interaction between molecules. The fingerprint plots were decomposed to highlight particularly close contacts between elements of the compound (Fig. 3). This decomposition could distinguish contributions from different interaction types, which overlap in the full fingerprint. The H···H interaction was one of the most significant contacts for **TMP-Cu** and **TMP-Co** (the percentage of H···H contacts was 41.9% and 42.4% for **TMP-Cu** and **TMP-Co**, respectively). It must be noted that O—H···N hydrogen bonds were observed in **TMP-Cu** and **TMP-Co** (the percentage of N···H contacts of **TMP-Cu** and **TMP-Co** was 19.8% and 21.8%, respectively). In addition, another main intermolecular interaction of **TMP-Cu** and **TMP-Co** was O···H contacts, which were represented by a scissors of the fingerprint plot (the percentage of O···H contacts was 11.5% and 10.9% for **TMP-Cu** and **TMP-Co**, respectively). Further, the π···π contacts played important roles in the 2-D fingerprint plot. The percentage of C···C contacts of **TMP-Cu** and **TMP-Co** was 4.4% and 5.0%, respectively. Apart from those above, the presence of C···H, M···H and other contacts was observed, and they are all summarized in Fig. 4. The interaction molecules were analyzed by the Hirshfeld surface and fingerprint plot, which showed similarity with the result of the single crystal X-ray diffraction.

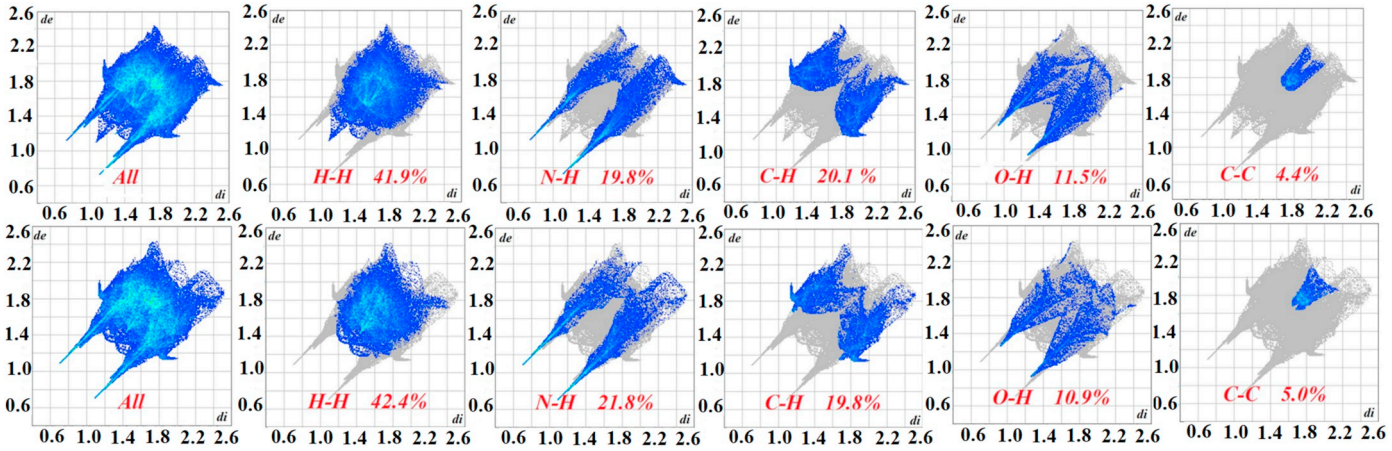

Fig. 3. Fingerprint plots: all, H···H, N···H, C···H, O···H and C···C contacts showing the percentages of contacts contributed to the total Hirshfeld surface area of **TMP-Cu** (top) and **TMP-Co** (down).

2.3. Cytotoxicity

The cytotoxic activity of H-TMP, $CuCl_2{\cdot}2H_2O$, cisplatin, **TMP-Cu** and **TMP-Co** complexes was examined in Hep-G2, NCI-H460, MGC80-3, BEL-7404 and HL-7702 cell lines. Results of MTT assay were presented as IC_{50} (μM) values for each compound after 48 h of treatment (Table 1). Against all selected human cell lines, **TMP-Cu** and **TMP-Co** exhibited the strongest cytotoxic effect against Hep-G2 cancer cells, after 48 h of exposure with IC_{50} values of 1.08 ± 0.38 μM and 15.06 ± 1.13 μM, respectively. However, the cytotoxic effect was significantly lower against normal HL-7702 cells (IC_{50} > 80 μM). Therefore, **TMP-Cu** and **TMP-Co** showed greater selective cytotoxicity towards Hep-G2 cancer cells after 48 h treatment, in comparison with the standard drug cisplatin [30–33]. Most notably, **TMP-Cu** (IC_{50} = 1.08 ± 0.38 μM) was about 60-fold, 15-fold, and 13-fold more potent than H-TMP, **TMP-Co**, and cisplatin against Hep-G2 cancer cells (IC_{50} values of 60.18 ± 0.49, 15.06 ± 1.13, and 13.87 ± 1.09 μM, respectively), which deserve further determination. In addition, the bond length of Cu1—O3, which was 2.483(2) Å, was a very weak coordination bond in the **TMP-Cu** complex. In solvent, the $[M(TMP)_2(H_2O)_2]$ may decompose $[M(TMP)_2]$, which reduced O—H···N hydrogen bond interactions and activated $[M(TMP)_2]$ to attack the human tumor cells.

2.4. *TMP-Cu* and *TMP-Co* induced cell cycle arrest through regulation of S phase related protein expressions

It is well known that most of anticancer compounds induce cell apoptosis via induction of cell cycle arrest [34–36]. As illustrated in Fig. 5, incubation of Hep-G2 cancer cells with **TMP-Cu** (1.0 μM) and **TMP-Co** (15.0 μM) increased the percentage of cells in the S phase from 32.59% to 46.16% (and 37.39%), whereas the percentage of cells in G2/M phase decreased concomitantly. Thus, the above results of the cell cycle analysis assay indicate that **TMP-Cu** (1.0 μM) and **TMP-Co** (15.0 μM) induce Hep-G2 cancer cell cycle arrest at the S phase.

To obtain insight into the mechanism of **TMP-Cu** (1.0 μM) and **TMP-Co** (15.0 μM) in Hep-G2 cell cycle arrest at the S phase, Western Blotting assay was performed to determine the expression of cdk2, p53, cyclin A, p21 and p27 proteins [34–36]. As shown in Fig. 6, **TMP-Cu** (1.0 μM) and **TMP-Co** (15.0 μM) induced S phase arrest in Hep-G2 cancer cells, decreased cdk2 and cyclin A protein levels, and increased expression of p53, p21 and p27. These data suggest that the **TMP-Cu** (1.0 μM) and **TMP-Co** (15.0 μM)-induced S arrest may be associated with regulation of S phase related protein expressions. Based on the western blot and agarose gel electrophoresis assay (Figs. 6 and S2), we can conclude that **TMP-Cu** (1.0 μM) with DNA most probably acted via an intercalation to significantly induce DNA damage (over-expression of 53BP1 protein) than **TMP-Co** (15.0 μM) in Hep-G2 cells [33–36]. In general, these results indicate that **TMP-Cu** (1.0 μM) and **TMP-Co** (15.0 μM) remarkably DNA damage, especially for **TMP-Cu** (1.0 μM) treated cancer cells, consequently causing cell cycle arrest at S phase (Figs. 5, 6, and S2).

2.5. *TMP-Cu* and *TMP-Co* induced cancer cell apoptosis

Considering that cell cycle arrest at the S phase will eventually lead

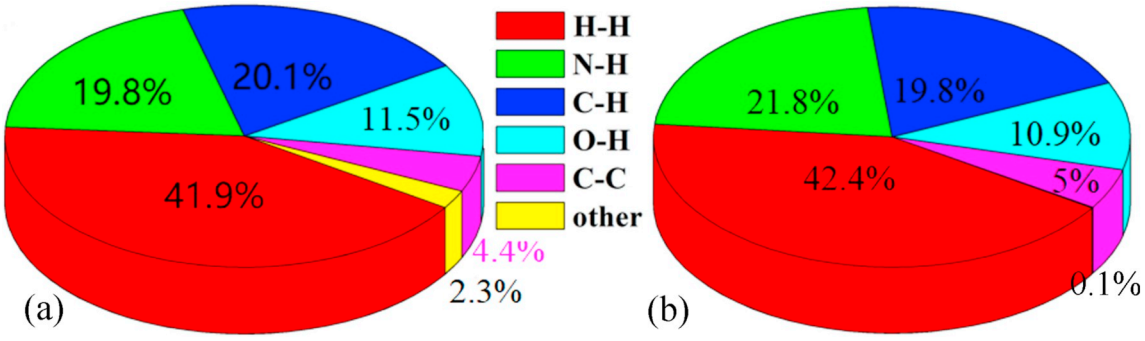

Fig. 4. Fingerprint plots: H···H, N···H, C···H, O···H, C···C and other bonds contacted showing the percentages of contacts contributed to the total Hirshfeld surface area of **TMP-Cu** (a) and **TMP-Co** (b).

Table 1
IC_{50} (μM) values determined by MTT assay of H-TMP, $CuCl_2{\cdot}2H_2O$, cisplatin, **TMP-Cu** and **TMP-Co** complexes against Hep-G2, NCI-H460, MGC80-3, BEL-7404 and HL-7702 human cell lines for 48 h.

Compounds	Hep-G2	NCI-H460	MGC80-3	BEL-7404	HL-7702
H-TMP	60.18 ± 0.49	> 100	> 100	> 100	70.24 ± 1.15
TMP-Cu	1.08 ± 0.38	87.47 ± 1.56	18.21 ± 1.58	65.55 ± 0.38	81.61 ± 0.78
TMP-Co	15.06 ± 1.13	> 100	25.09 ± 0.85	19.01 ± 1.72	> 100
$CuCl_2{\cdot}2H_2O$	> 150	> 100	> 150	> 100	> 100
Cisplatin	13.87 ± 1.09	17.02 ± 2.11	15.02 ± 1.99	18.54 ± 1.24	16.01 ± 1.23

to cell apoptosis [37,38], after incubated with **TMP-Cu** (1.0 μM) and **TMP-Co** (15.0 μM) for 24 h, the Hep-G2 cancer cells were stained by Annexin V-FITC (FITC is fluorescein isothiocyanate) and PI (propidium iodide), and examined by flow cytometry. As shown in Fig. 7, the percentage of **TMP-Cu** (1.0 μM) and **TMP-Co** (15.0 μM) promoting cell apoptosis (early and late apoptosis) was 20.76% and 11.14%, respectively. These results also suggested that **TMP-Cu** (1.0 μM) was more effective in promoting cell apoptosis than **TMP-Co** (15.0 μM).

2.6. *TMP-Cu and TMP-Co induced cancer cell mitochondrial dysfunction*

First, to study the cellular uptake of **TMP-Cu** (1.0 μM) and **TMP-Co** (15.0 μM) in these Hep-G2 cells, an ICP-MS assay was carried out [23,32,39–43]. As shown in Fig. 8 and Table S1, the maximum intake of **TMP-Cu** (1.0 μM) was higher ((95.06 ± 0.85 ng Cu)/10^6 cells) than that of **TMP-Co** (15.0 μM) ((54.45 ± 0.46 ng Co)/10^6 cells) and cisplatin [23,32], which was mainly distributed in the mitochondria fractions. The result suggests that a Cu ion in the **TMP-Cu** complex might promote its effect on cell intake [23,32,39–43], which has been proven in this study by examining the metal (Cu or Co) intake and distribution of **TMP-Cu** and **TMP-Co** using the ICP-MS method. This may be the most plausible explanation for the better antitumor effect of **TMP-Cu** compared to **TMP-Co** based on the present results. In addition, it has been found that mitochondrial dysfunction, including reduction of mitochondrial membrane potential (MMP, Δψ), intracellular Ca^{2+}, and ROS (reactive oxygen species) levels, is closely connected with cell apoptosis [44–49]. Thus, the capacity of **TMP-Cu** (1.0 μM) and **TMP-Co** (15.0 μM) to reduce of MMP, intracellular Ca^{2+}, and ROS levels in Hep-G2 cancer cells was assess using flow cytometry. In comparison with control cells, **TMP-Cu** (1.0 μM) and **TMP-Co** (15.0 μM) treated groups

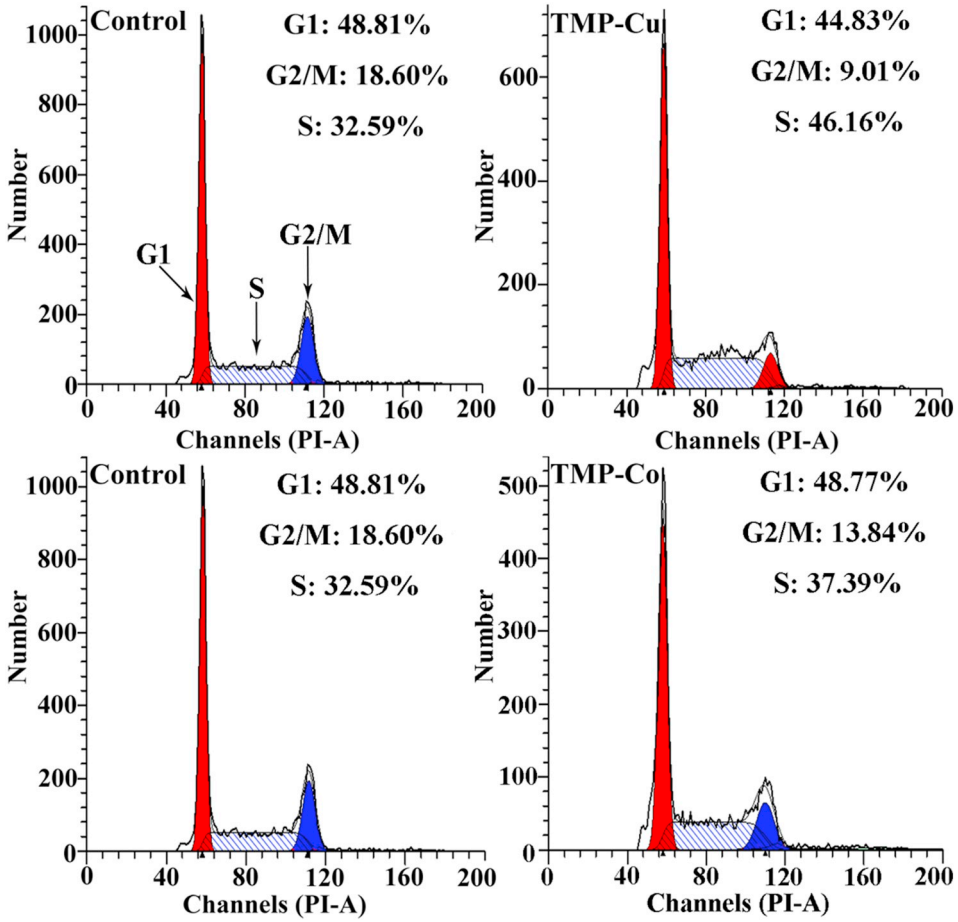

Fig. 5. TMP-Cu (1.0 μM) and **TMP-Co** (15.0 μM) induced S phase arrest in Hep-G2 cancer cells for 24 h.

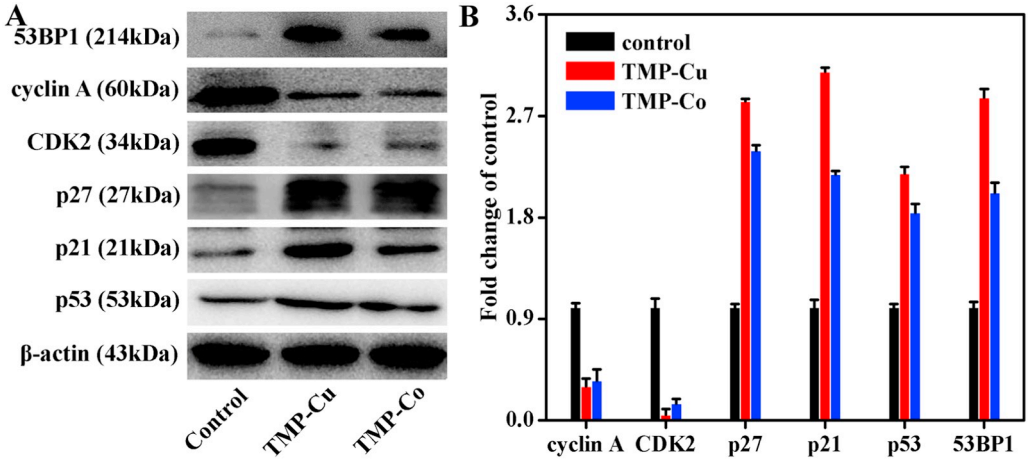

Fig. 6. (A) Western blotting assay of **TMP-Cu** (1.0 μM) and **TMP-Co** (15.0 μM) on the S phase regulatory proteins in Hep-G2 cancer cells for 24 h. (B) Histograms display the density ratios of cdk2, p53, cyclin A, p21, 53BP1 and p27 to β-actin.

resulted in increased levels of Ca^{2+} and ROS, and decreased MMP (Fig. 9), suggesting that MMP, Ca^{2+}, and ROS play a vital role in **TMP-Cu** and **TMP-Co** induced cell death [44–49].

To further demonstrate the mitochondrial pathways in Hep-G2 cell apoptosis induced by **TMP-Cu** (1.0 μM) and **TMP-Co** (15.0 μM), Western blotting analysis was performed [44–51]. As shown in Fig. 10, treatment with **TMP-Cu** (1.0 μM) and **TMP-Co** (15.0 μM) decreased expression of the Bcl-2 protein and increased expression of the caspase-3/-9, apaf-1, bax, and cyt c (cytochrome *c*) protein levels, suggesting that the mitochondrial pathway was involved in Hep-G2 cancer cell apoptosis driven by **TMP-Cu** (1.0 μM) and **TMP-Co** (15.0 μM).

3. Conclusions

In this study, two transition metal **TMP-Cu** and **TMP-Co** complexes of (*E*)-2-(((4H-1,2,4-triazol-4-yl)imino)methyl)-6-methoxyphenol (H-TMP) were synthesized and characterized. The structures of **TMP-Cu** and **TMP-Co** were determined by X-ray crystallography, IR, and elemental analysis. MTT assay showed that **TMP-Cu** display stronger antiproliferative activity towards the Hep-G2 cancer cell line than **TMP-Co**, cisplatin and H-TMP. Interestingly, **TMP-Cu** and **TMP-Co** exhibited low cytotoxicity against normal HL-7702 cells. Furthermore, **TMP-Cu** and **TMP-Co** arrested the cell cycle at S phase through regulation of S phase related proteins expression in the Hep-G2 cells. Mechanism studies showed that **TMP-Cu** and **TMP-Co** induced cell apoptosis was associated with mitochondrial dysfunction in Hep-G2 cancer cells. Our reported studies imply that a Cu ion in the **TMP-Cu** complex might promote its effect on cell intake, which has been proven in this study by examining the metal (Cu or Co) intake and distribution of **TMP-Cu** and **TMP-Co** using the ICP-MS method. Therefore, this may be the most plausible explanation for the better antitumor effect of **TMP-Cu** compared to **TMP-Co** based on the present results.

4. Experimental

4.1. Materials and physical measurements

All chemicals were commercially available and used as received without purification. Elemental analyses (CHN) were performed using a Perkin-Elmer 240 elemental analyzer. FT-IR spectra were recorded from KBr pellets in the range of 4000–400 cm^{-1} on a Bio-Rad FTS-7 spectrometer. The X-ray crystal structures were determined by Agilent G8910A CCD diffractometer using the SHELXL crystallographic software for molecular structures. Photo-luminescents tested by Hitachi F-4600 fluorescence spectrophotometer.

4.2. Syntheses

4.2.1. Syntheses of H-TMP

A mixture of 2-Hydroxy-3-methoxy-benzaldehyde (10 mmol, 1.520 g), 4-amino-1,2,4-triazole (Hatz, 10 mmol, 0.8408 g) and ethanol (20 mL) in a 100 mL flask refluxed at 80 °C for 2 h. Beige precipitate

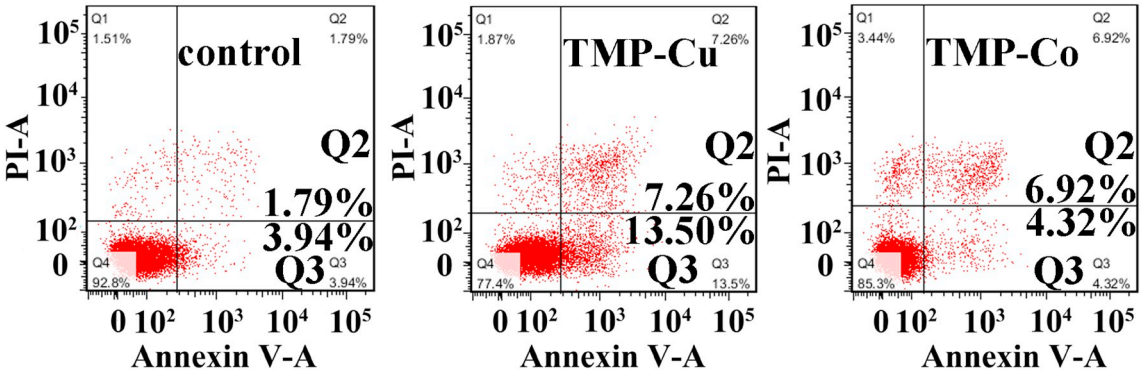

Fig. 7. Double staining on the Hep-G2 tumor cells treated by **TMP-Cu** (1.0 μM) and **TMP-Co** (15.0 μM) for 24 h.

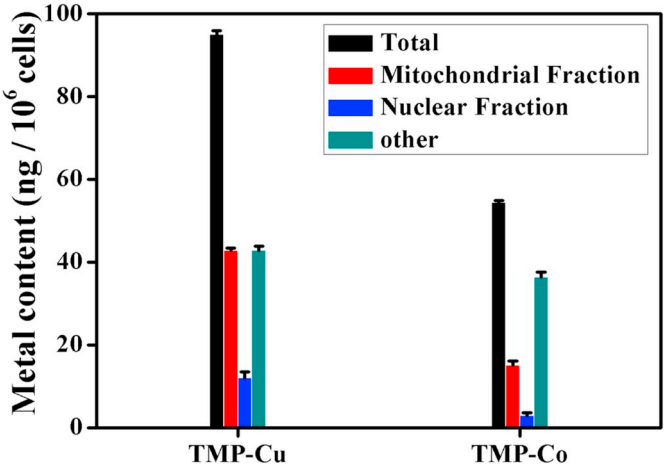

Fig. 8. The cellular uptake and different fractions of **TMP-Cu** (1.0 μM) and **TMP-Co** (15.0 μM) in Hep-G2 cells.

appeared and then was rinsed three times with fresh ethanol (5 mL × 3) and dried at 40 °C for 12 h (yield ≈95% based on Hatz). *Anal. Calc.* for H-TMP: $C_{10}H_{10}N_4O_2$ (M_r = 218.18), *calc.*: C, 55.05; H, 4.62; N, 25.67%; Found: C, 55.01; H, 4.65; N, 25.72. IR data for H-TMP (KBr, cm^{-1}, Fig. S3): 3430 m, 3089 s, 1594 s, 1529 m, 1476 s, 1443 s, 1238 s, 1156 s, 1071 s, 971 w, 929 w, 730 w, 627 w.

4.2.2. *[Cu(TMP)$_2$(H$_2$O)$_2$] (**TMP-Cu**)*

A mixture of $Cu(Ac)_2{\cdot}H_2O$ (0.2 mmol, 0.040 g), H-TMP (0.2 mmol, 0.044 g), DMF (5 mL), acetonitrile (5 mL) and deionized water (1 mL) was sealed in a 20 mL vial at 80 °C for 72 h. Dark green block crystals of **TMP-Cu** were collected by filtration, washed with deionized water (10 mL × 3) and dried in air (yield: 31 mg, ca. 58.3% based on H-TMP). *Anal. Calc.* for **TMP-Cu**: $C_{20}H_{22}N_8O_6Cu$ (M_r = 534.01), *calc.*: C, 44.98; H, 4.15; N, 20.97. Found: C, 45.02; H, 4.20; N, 21.03. IR data for **TMP-Cu** (KBr, cm^{-1}, Fig. S4): 3442 m, 3084 s, 2953 w, 1605 s, 1540 m, 1443 s, 1232 m, 1115 s, 1052 s, 987 m, 883 s, 746 m, 648 w, 590 w.

4.2.3. *[Co(TMP)$_2$(H$_2$O)$_2$] (**TMP-Co**)*

Complex **TMP-Co** was prepared in a similar way to **TMP-Cu**, except that $Cu(Ac)_2{\cdot}H_2O$ was replaced by $Co(Ac)_2{\cdot}2H_2O$. Red block crystals of **TMP-Co** were collected by filtration, washed with deionized water (10 mL × 3) and dried in air (yield: 30 mg, ca. 56.9% based on H-TMP). *Anal. Calc.* For **TMP-Co**: $C_{20}H_{22}N_8O_6Co$ (*Mr* = 529.39), *calc.*: C, 45.37; H, 4.19; N, 21.16%. Found: C, 45.43; H, 4.16; N, 21.21%. IR data for **TMP-Co** (KBr, cm^{-1}, Fig. S5):3430 m, 3089 s, 1594 s, 1529 m, 1443 s, 1238 m, 1101 s, 1043 s, 971 m, 899 w, 742 s, 643 w, 565 w.

4.3. X-ray crystallography

Two diffraction data were collected on Agilent G8910A CCD diffractometer with graphite monochromated Mo-Kα radiation (λ = 0.71073 Å) and using the ω-θ scan mode in the ranges $2.91^\circ \le \theta \le 25.08^\circ$(**TMP-Cu**), and $2.96^\circ \le \theta \le 25.10^\circ$(**TMP-Co**) respectively. Raw frame data were integrated with the SAINT program [52]. The structures were solved by direct methods using SHELXS-97 and refined by full-matrix least-squares on F^2 using SHELXS-97 [52]. An empirical absorption correction was applied with the program CrysAlis RED (Agilent, 2012). All non-hydrogen atoms were refined anisotropically. All hydrogen atoms were positioned geometrically and refined as riding. Calculations and graphics were performed with SHELXTL [52]. The crystallographic details are provided in Table S2. Selected bond distances and angles of the **TMP-Cu** and **TMP-Co** are listed in Table S3. Crystallographic data for the structural analysis have been deposited with the Cambridge Crystallographic Data Center (CCDC reference numbers: 1876582, 1876583).

4.4. Materials and methods

The anticancer mechanism of **TMP-Cu** (1.0 μM) and **TMP-Co** (15.0 μM) was studied according to Ulukaya and Chao et al. reported [44–51]. In addition, the detailed procedures for the anticancer mechanism of **TMP-Cu** (1.0 μM) and **TMP-Co** (15.0 μM) in Hep-G2 cancer cells were described in supporting information.

Abbreviations

PBS	phosphate buffer saline
MTT	3-(4,5-dimethylthiazol-2-yl)-2,5-diphenyltetrazolium bromide
IC_{50}	half maximal inhibitory concentration
ROS	reactive oxygen species
Hep-G2 cells	human hepatocellular carcinoma cells
NCI-H460 cells	human non-small cell lung cancer cells
MGC 80-3 cells	human gastric adenocarcinoma cell line
BEL-7404 cells	human hepatocarcinoma cell line
HL-7702 cells	human normal hepatocytes cells
FITC	fluorescein isothiocyanate
PI	propidium iodide
MMP	mitochondrial membrane potential

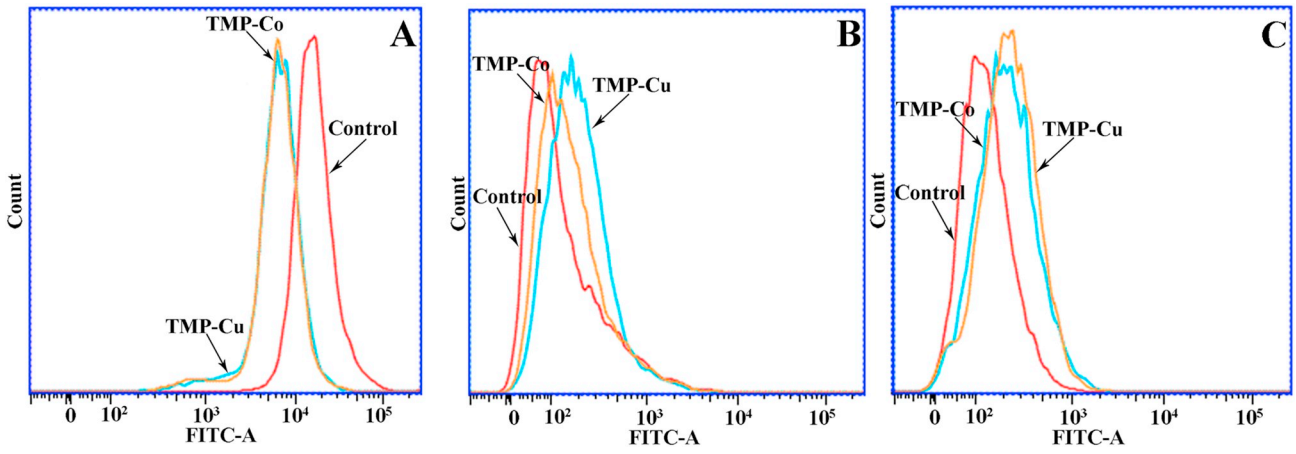

Fig. 9. Effects of **TMP-Cu** (1.0 μM) and **TMP-Co** (15.0 μM) on MMP (A), Ca^{2+} (B) and ROS (C) levels in the Hep-G2 cancer cells analyzed by flow cytometry.

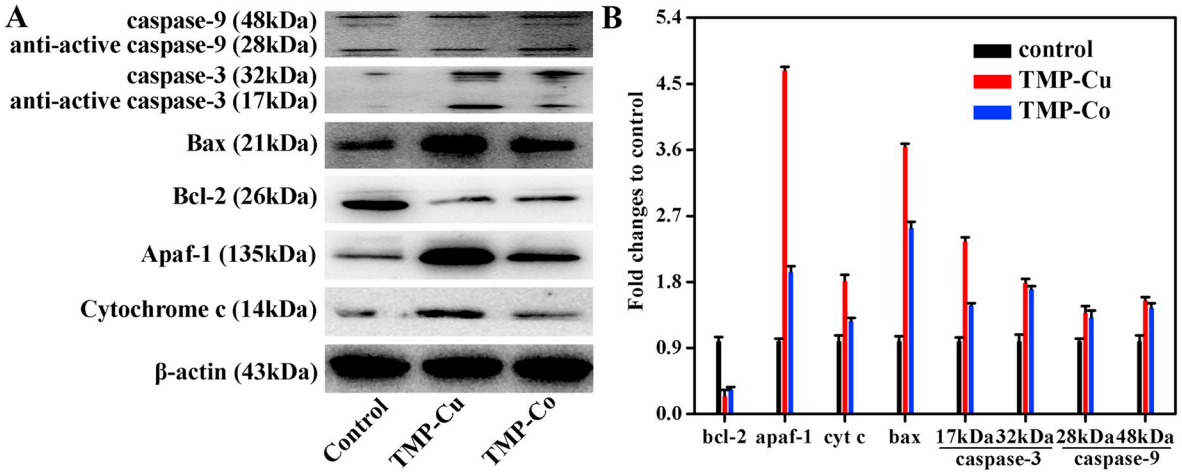

Fig. 10. (A) Western blotting analysis of bcl-2, caspase-3/-9, apaf-1, bax and cyt c induced by **TMP-Cu** (1.0 μM) and **TMP-Co** (15.0 μM) in Hep-G2 cells. (B) Histograms display the density ratios of bcl-2, caspase-3/-9, apaf-1, bax and cyt c to β-actin.

Acknowledgments

This work was supported by the Natural Science Foundation of China (No. 21861014, 21867017 and 21761033), the Program of the Collaborative Innovation Center for Exploration of Hidden Nonferrous Metal Deposits and Development of New Materials in Guangxi (No. GXYSXTZX2017-II-3) as well as the Natural Science Foundation of Guangxi Province (No. 2018GXNSFBA138021).

Appendix A. Supplementary data

Electronic supplementary information (ESI) available: IR and crystal data for H-TMP, **TMP-Cu** and **TMP-Co**. CCDC Nos. 1876582 and 1876583 for **TMP-Cu** and **TMP-Co** contains the supplementary crystallographic data for this study. Supplementary data associated with this article can be found in the online version, at https://doi.org/10.1016/j.jinorgbio.2019.01.009. These data include MOL file and InChiKey of the most important compounds described in this article.

References

[1] L.H. Hurley, Nat. Rev. Cancer 2 (2002) 188–200.
[2] Q. Cao, Y. Li, E. Freisinger, P.Z. Qin, R.K.O. Sigel, Z.-W. Mao, Inorg. Chem. Front. 4 (2017) 10–32.
[3] O. Pinato, C. Musetti, C. Sissi, Metallomics 6 (2014) 380–395.
[4] H. Kostrhunova, J. Florian, O. Novakova, A.F.A. Peacock, P.J. Sadler, V. Brabec, J. Med. Chem. 51 (2008) 3635–3643.
[5] J.S. Butler, P.J. Sadler, Curr. Opin. Chem. Biol. 17 (2013) 175–188.
[6] Y. Chen, Z. Guo, S. Parsons, P.J. Sadler, Chem. Eur. J. 4 (2015) 672–676.
[7] W. Liu, X. Chen, M. Xie, L. Lou, Q. Ye, Y. Yu, S. Hou, J. Inorg. Biochem. 102 (2008) 1942–1946.
[8] Y. Zhao, G.M. Roberts, S.E. Greenough, N.J. Farrer, M.J. Paterson, W.H. Powell, V.G. Stavros, P.J. Sadler, Angew. Chem. Int. Ed. 51 (2012) 11263–11266.
[9] A.F. Westendorf, J.A. Woods, K. Korpis, N.J. Farrer, L. Salassa, K. Robinson, V. Appleyard, K. Murray, R. Grünert, A.M. Thompson, P.J. Sadler, P.J. Bednarski, Mol. Cancer Ther. 11 (2012) 1894–1904.
[10] J.S. Butler, J.A. Woods, N.J. Farrer, M.E. Newton, P.J. Sadler, J. Am. Chem. Soc. 134 (2012) 16508–16511.
[11] G.Y. Park, J.J. Wilson, Y. Song, S.J. Lippard, PNAS 109 (2012) 11987–11992.
[12] J.J. Wilson, S.J. Lippard, Chem. Rev. 114 (2014) 4470–4495.
[13] T. Zou, J. Liu, C.T. Lum, C. Ma, R.C.-T. Chan, C.-N. Lok, W.-M. Kwok, C.-M. Che, Angew. Chem. Int. Ed. 126 (2014) 10283–10287.
[14] P.C.A. Bruijnincx, P.J. Sadler, Curr. Opin. Chem. Biol. 12 (2008) 197–206.
[15] S.W. Ragsdale, J. Inorg. Biochem. 101 (2007) 1657–1666.
[16] X.Y. Qin, L.C. Yang, F.L. Le, Q.Q. Yu, D.D. Sun, Y.N. Liu, J. Liu, Dalton Trans. 42 (2013) 14681–14684.
[17] H.-Y. Zhang, W. Wang, H. Chen, S.-H. Zhang, Y. Li, Inorg. Chim. Acta 453 (2016) 507–515.
[18] S. Tardito, A. Barilli, I. Bassanetti, M. Tegoni, O. Bussolati, R. Franchi-Gazzola, C. Mucchino, L. Marchiò, J. Med. Chem. 55 (2012) 10448–10459.
[19] Q.P. Huang, S.N. Zhang, S.H. Zhang, K. Wang, Y. Xiao, Molecules 22 (2017) 1813.
[20] A. Paul, S. Anbu, G. Sharma, M.L. Kuznetsov, B. Koch, M. Fatima, C.G. da Silva, A.J.L. Pombeiro, Synthesis, Dalton Trans. 44 (2015) 19983–19996.
[21] Q.Q. Zhang, F. Zhang, W.G. Wang, X.L. Wang, J. Inorg. Biochem. 100 (2006) 1344–1352.
[22] X. Qiao, Z.Y. Ma, C.Z. Xie, F. Xue, Y.W. Zhang, J.Y. Xu, S.P. Yan, J. Inorg. Biochem. 105 (2011) 728–737.
[23] Q.-P. Qin, T. Meng, M.-X. Tan, Y.-C. Liu, X.-J. Luo, B.-Q. Zou, H. Liang, Eur. J. Med. Chem. 143 (2018) 1597–1603.
[24] G. Turan-Zitouni, Z.A. Kaplancıklı, M.T. Yıldız, P. Chevallet, D. Kaya, Eur. J. Med. Chem. 40 (2005) 607–613.
[25] S.H. Zhang, J. Wang, H.-Y. Zhang, Y. Fan, Y. Xiao, Dalton Trans. 46 (2017) 410–419.
[26] Y.M. Chen, Q. Gao, H.F. Zhang, D.D. Gao, Y.H. Li, W. Liu, W. Li, Polyhedron 71 (2014) 91–98.
[27] B.E. Applegate, T.A. Barckholtz, T.A. Miller, Chem. Soc. Rev. 32 (2003) 38–49.
[28] M.A. Halcrow, Chem. Soc. Rev. 42 (2013) 1784–1795.
[29] S.H. Zhang, R.-X. Zhao, G. Li, H.-Y. Zhang, Q.-P. Huang, F.-P. Liang, J. Solid State Chem. 220 (2014) 206–212.
[30] D. Ćoćić, S. Jovanović, S. Radisavljević, J. Korzekwa, A. Scheurer, R. Puchta, D. Baskić, D. Todorović, S. Popović, S. Matić, B. Petrović, J. Inorg. Biochem. 189 (2018) 91–102.
[31] Q.-P. Qin, S.-L. Wang, M.-X. Tan, Z.-F. Wang, X.-L. Huang, Q.-M. Wei, B.-B. Shi, B.-Q. Zou, H. Liang, Metallomics 10 (2018) 1160–1169.
[32] Q.-P. Qin, S.-L. Wang, M.-X. Tan, Z.-F. Wang, D.-M. Luo, B.-Q. Zou, Y.-C. Liu, P.-F. Yao, H. Liang, Eur. J. Med. Chem. 158 (2018) 106–122.
[33] Q.-P. Qin, Z.-F. Chen, J.-L. Qin, X.-J. He, Y.-L. Li, Y.-C. Liu, K.-B. Huang, H. Liang, Eur. J. Med. Chem. 92 (2015) 302–313.
[34] F.A.R. Barbosa, T. Siminski, R.F.S. Canto, G.M. Almeida, N.S.R.S. Mota, F. Ourique, R.C. Pedrosa, A.L. Braga, Eur. J. Med. Chem. 155 (2018) 503–515.
[35] Z.-F. Chen, Q.-P. Qin, J.-L. Qin, Y.-C. Liu, K.-B. Huang, Y.-L. Li, T. Meng, G.-H. Zhang, Y. Peng, X.-J. Luo, H. Liang, J. Med. Chem. 58 (2015) 2159–2179.
[36] S. Xu, H. Yao, S. Luo, Y.-K. Zhang, D.-H. Yang, D. Li, G. Wang, M. Hu, Y. Qiu, X. Wu, H. Yao, W. Xie, Z.-S. Chen, J. Xu, J. Med. Chem. 60 (2017) 1449–1468.
[37] M.I. Khan, A. Mohammad, G. Patil, S.A. Naqvi, L.K. Chauhan, I. Ahmad, Biomaterials 33 (2012) 1477–1488.
[38] J. Qi, Q. Yao, L. Tian, Y. Wang, Eur. J. Med. Chem. 158 (2018) 853–862.
[39] N. Yamamoto, A.K. Renfrew, B.J. Kim, N.S. Bryce, T.W. Hambley, J. Med. Chem. 55 (2012) 11013–11021.
[40] P.D. Bonnitcha, B.J. Kim, R.K. Hocking, J.K. Clegg, P. Turner, S.M. Neville, T.W. Hambley, Dalton Trans. 41 (2012) 11293–11304.
[41] B.P. Green, A.K. Renfrew, A. Glenister, P. Turner, T.W. Hambley, Dalton Trans. 46 (2017) 15897–15907.
[42] J.Z. Zhang, E. Wexselblatt, T.W. Hambley, D. Gibson, Chem. Commun. 48 (2018) 847–849.
[43] E. Wexselblatt, D. Gibson, J. Inorg. Biochem. 117 (2012) 220–229.
[44] L.M. Chen, F. Peng, G.D. Li, X.M. Jie, K.R. Cai, C. Cai, Y. Zhong, H. Zeng, W. Li, Z. Zhang, J.C. Chen, J. Inorg. Biochem. 156 (2016) 64–74.
[45] X.-D. Song, X. Kong, S.-F. He, J.-X. Chen, J. Sun, B.-B. Chen, J.-W. Zhao, Z.-W. Mao, Eur. J. Med. Chem. 138 (2017) 246–254.
[46] Q.-P. Qin, S.-L. Wang, M.-X. Tan, Y.-C. Liu, T. Meng, B.-Q. Zou, H. Liang, Eur. J. Med. Chem. 161 (2019) 334–342.

[47] V.T. Yilmaz, C. Icsel, M. Aygun, M. Erkisa, E. Ulukaya, Eur. J. Med. Chem. 158 (2018) 534–547.
[48] C. Icsel, V.T. Yilmaz, M. Aygun, B. Cevatemre, P. Alperd, E. Ulukaya, Dalton Trans. 47 (2018) 11397–11410.
[49] D. Wan, B. Tang, Y.-J. Wang, B.-H. Guo, H. Yin, Q.-Y. Yi, Y.-J. Liu, Eur. J. Med. Chem. 139 (2017) 180–190.
[50] H.-H. Zou, L. Wang, Z.-X. Long, Q.-P. Qin, Z.-K. Song, T. Xie, S.-H. Zhang, Y.-C. Liu, B. Lin, Z.-F. Chen, Eur. J. Med. Chem. 108 (2016) 1–12.
[51] H.-Y. Huang, P.-Y. Zhang, B.-L. Yu, Y. Chen, J.-Q. Wang, L.-N. Ji, H. Chao, J. Med. Chem. 57 (2014) 8971–8983.
[52] G.M. Sheldrick, Acta Cryst C71 (2015) 3–8.